Performance analysis of a miniature Joule–Thomson cryocooler with and without the distributed J–T effect

Rashmin Damle and Milind Atrey

Department of Mechanical Engineering, Indian Institute of Technology Bombay, Powai, Mumbai 400076, Maharashtra, India

E-mail: matrey@iitb.ac.in

Abstract. Cryogenic temperatures are obtained with Joule–Thomson (J–T) cryocoolers in an easier way as compared to other cooling techniques. Miniature J–T cryocoolers are often employed for cooling of infrared sensors, cryoprobes, biological samples, etc. A typical miniature J–T cryocooler consists of a storage reservoir/compressor providing the high pressure gas, a finned tube recuperative heat exchanger, an expansion valve/orifice, and the cold end. The recuperative heat exchanger is indispensable for attaining cryogenic temperatures. The geometrical parameters and the operating conditions of the heat exchanger drastically affect the cryocooler performance in terms of cool down time and cooling effect. In the literature, the numerical models for the finned recuperative heat exchanger have neglected the distributed J–T effect. The distributed J–T effect accounts for the changes in enthalpy of the fluid due to changes of pressure in addition to those due to changes of temperature. The objective of this work is to explore the distributed J–T effect and study the performance of a miniature J–T cryocooler with and without the distributed J–T effect. A one dimensional transient model is employed for the numerical analysis of the cryocooler. Cases with different operating conditions are worked out with argon and nitrogen as working fluids.

1. Introduction

Cooling to cryogenic temperatures using Joule–Thomson (J–T) effect is a well known technology. J–T cryocoolers have advantages like: simple design; no moving parts; high reliability; low maintenance; and low cost. It can also have fast cool down time if required as compared to other cryocoolers. Moreover, the possibility of miniaturization is well suited for applications like thermal cameras, cryosurgery probes, cooling of infrared sensors, etc. The most critical element of such cryocoolers is the counter-flow recuperative heat exchanger. The recuperative heat exchanger, typically of Hampson type as shown in Figure 1, consists of a finned tube wound over a mandrel core and a covering shield forming an outer annulus. In an open cycle mode, the high pressure gas flows through the finned tube, expands through an expansion device, and flows over the outer surface of the finned tube on its way out. This forms a counter-flow recuperative heat exchanger. Usually, the high pressure gas enters the finned tube (hot side of the heat exchanger) at a pressure in the range of 100–400 bar depending on the working fluid. The temperature at the inlet is close to the ambient temperature (300 K). The gas in the helical finned tube experiences a very high pressure drop along with heat transfer. The return gas in the external annulus (cold side of the heat exchanger) enters at low pressure around 1.5–2 bar

and at a temperature of about 80–110 K. The geometrical configuration of the heat exchanger and the working conditions (i.e., mass flow rates and inlet pressure) drastically affect the cool down characteristics in terms of cooling capacity and cool down time. A parametric study is therefore useful for optimization of cryocooler performance.

Many researchers have studied miniature J–T cryocoolers. Xue et al. [1] and Ng et al. [2] carried out both experimental and numerical analyses on a miniature J-T cryocooler. Chua et al. [3], Hong et al. [4] and Ardhapurkar and Atrey [5] focussed on the steady state analysis of the recuperative heat exchanger. Chou et al. [6], Chien et al. [7], Hong et al. [8] and Hong et al. [9] studied the transient behaviour of miniature J–T cryocoolers. Maytal [10] suggested that the pressure drop along the length of the high pressure side causes a distributed J–T expansion effect and any additional expansion device at the end of the tube can thus be eliminated. The above studies have neglected this distributed J–T effect along the length of the high pressure side. Recently, Damle and Atrey [11] investigated the distributed J–T effect and showed that it cannot be neglected when the pressure drop on the high pressure side is large.

The aim of this work is to explore the distributed J–T effect and its influence on the transient performance of the cryocooler. A one-dimensional transient model validated previously by Damle and Atrey [11] is used for doing the parametric analysis. Numerical simulations with different working fluids and operating conditions are carried out to see their effect on the cool down time and cooling effect with and without the distributed J–T effect.

2. The distributed J–T effect

The distributed J–T effect produces a substantial temperature drop, even without wall heat transfer, when the pressure variation along the finned tube length is large. The same is demonstrated in Figure 2 reported by [11]. In this case, when the energy equation is resolved in terms of temperature by putting $dh = C_p dT$, there is no change in temperature as indicated by the constant temperature line. However, when the distributed J–T effect is considered by putting $dh = C_p dT - \mu_{JT} C_p dp$, the fluid temperature reduces from 290 K to around 260 K due to the pressure drop (around 90 bar) along the length of the finned tube. The latter matches exactly with the curve obtained by solving the energy equation in terms of enthalpy (h) along

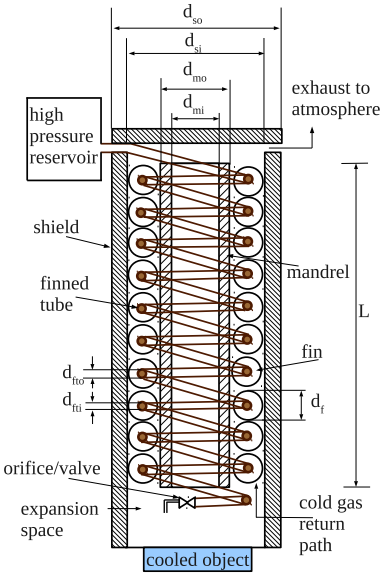

Figure 1. Cryocooler schematic.

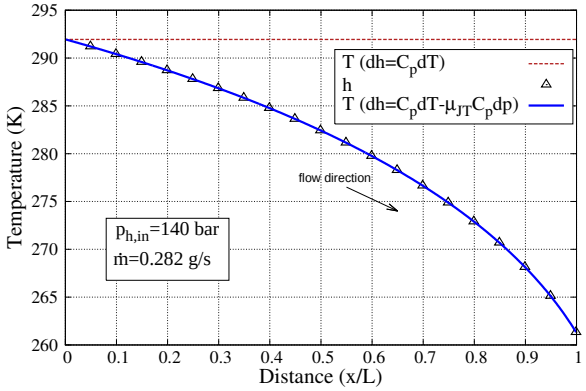

Figure 2. Temperature of the fluid along the finned tube with no wall heat transfer.

the finned tube length. Thus, the energy equation solved in terms of enthalpy takes care of the distributed J–T effect intrinsically. In all the cases, the physical properties (e.g., ρ, C_p, k, etc.) vary with temperature and pressure along the fluid length. It should be noted that when the distributed J–T effect is considered, the changes in enthalpy and in turn those in temperature due to changes of pressure are also taken in to account according to equation (1) suggested by Maytal [10]. The contribution of pressure variation, represented by the second term of the above equation, is neglected by several researchers. Thus, the changes in enthalpy due to changes of temperature alone have been taken into account.

$$dh = C_p dT - \mu_{JT} C_p dp \tag{1}$$

3. Mathematical model

A one-dimensional transient model is employed for the simulation of the fluid streams and the solid elements (i.e., finned tube, mandrel and shield) which together form the heat exchanger. The different elements of the heat exchanger are divided into a series of control volumes (CVs) over which the governing equations are solved. A brief description of the transient numerical model previously detailed in [11] is presented in this section.

3.1. Governing equations

The basic equations of conservation of mass, momentum and energy for the fluid elements and energy conservation equation for solid elements are written in a differential form. The conservation of mass over a fluid CV is:

$$A\frac{\partial \bar{\rho}}{\partial t} + \frac{\partial \dot{m}}{\partial x} = 0 \tag{2}$$

The conservation of momentum is given by:

$$A\frac{\partial (\bar{\rho}\bar{V})}{\partial t} + \frac{\partial (\dot{m}V)}{\partial x} = -\frac{\partial p}{\partial x} \cdot A - \tau_w l_p \tag{3}$$

The energy equation in terms of enthalpy is written as:

$$A\frac{\partial (\bar{\rho}\bar{h})}{\partial t} + \frac{\partial (\dot{m}h)}{\partial x} = \alpha \cdot l_p \cdot (T_w - \bar{T}) \tag{4}$$

where, ρ=density (kg/m^3), A=cross-sectional area (m^2), V=velocity (m/s), $\dot{m}$=mass flow rate (kg/s), p=pressure (N/m^2), T=temperature (K), T_w=wall temperature, h=enthalpy (J/kg), α=heat transfer coefficient, $\tau_w = f\rho \mathrm{V}^2/2$ is the wall shear stress (N/m^2), f=Fanning friction factor, l_p=wetted perimeter (m), x= cartesian co-ordinate and t=time (s). Overbar on a variable represents the average over the given CV. The heat transfer coefficient and friction factor correlations are estimated as given in [2] and [6] . A general energy equation for the solid elements is the following:

$$\rho A C_p \frac{\partial T}{\partial t} = \frac{\partial}{\partial x}\left(kA\frac{\partial T}{\partial x}\right) + \dot{Q}_{conv} + \dot{Q}_{rad} \tag{5}$$

where, k=thermal conductivity (W/mK) and C_p=specific heat (J/kgK).Radiative heat transfer is calculated only for the outer surface of the shield. $\dot{Q}_{conv}$ represents the heat transfer per unit length due to convection from the surfaces of the solid elements. $\dot{Q}_{rad}$ is the heat transfer per unit length due to radiation considered only for the outer shield surface.

3.2. Boundary conditions

The boundary conditions of temperature (T), pressure (p) and mass flow rate ($\dot{m}$) are given at the inlet cross-section of the finned tube as in equation (6). The same are known at the inlet of the external annulus for the return gas and are given according to equation (7).

$$at\ x = 0\ \&\ t > 0\ :\ T = T_{h,in},\ p = p_{h,in},\ \frac{dT_w}{dx} = 0,\ \frac{dT_m}{dx} = 0,\ \frac{dT_s}{dx} = 0 \tag{6}$$

$$at\ x = L\ \&\ t > 0\ :\ T = T_{a,e},\ p = p_{c,in},\ \frac{dT_w}{dx} = 0,\ \frac{dT_m}{dx} = 0,\ \frac{dT_s}{dx} = 0 \tag{7}$$

The subscript in denotes inlet while subscripts h and c refer to the hot and cold side of the heat exchanger respectively. The subscripts w, m and s indicate the solid elements finned tube, mandrel and shield respectively. T_{ae} is the temperature of the gas after isenthalpic expansion, from its state at the exit of the finned tube, to the pressure $p_{c,in}$ at the inlet of external annulus. T_{ae} reduces from its initial value (ambient temperature) to cryogenic temperature $T_{c,in}$ at steady state. The minimum value of $T_{c,in}$ at steady state is fixed to 110 K. The cooling effect is calculated at steady state when the temperature of the gas after expansion falls below the $T_{c,in}$ value. All the solid elements (i.e., finned tube, mandrel and shield) are assumed to be adiabatic at ends. In addition, the initial temperature map for all the solid and fluid elements and pressure map for the fluid elements are specified as in equation (8).

$$at\ t = 0\ \&\ 0 \leq x \leq L\ :\ T = T_{amb},\ p = p_{c,in} \tag{8}$$

4. Results and discussion

In this work, all the cases have been simulated with the geometrical configuration of Xue et al. [1]. The effect of operating parameters like mass flow rate ($\dot{m}$) and supply pressure ($p_{h,in}$) on the cryocooler performance is studied. The simulations are carried out with both argon and nitrogen as working fluids with and without considering the distributed J–T effect. In both cases, at any given instant, the thermo-physical properties (e.g., ρ, C_p, k, etc.) are calculated at the temperature and pressure of the respective CV. The numerical model [11] used for analysis has been previously verified with mesh independence exercises and validated with the available experimental data. The properties of argon and nitrogen as a function of temperature and pressure are obtained from the commercial software AspenONE[12].

4.1. Effect of mass flow rate on the distributed J–T effect

Figures 3a and 3b illustrate the effect of mass flow rate on the distributed J–T effect reported earlier by Damle and Atrey [13]. They show, respectively, the pressure and temperature profiles along the length of the finned tube with high pressure gas for two different mass flow rates namely 0.37 g/s and 0.1 g/s. Both cases, are shown with and without the distributed J–T effect. A mass flow rate of 0.37 g/s represents a close to choking condition, while 0.1 g/s is chosen to be almost four times smaller than the choking value. The profiles obtained with the distributed J–T effect are indicated with "μ_{JT}". The inlet pressure and temperature for this case are 180 bar and 298 K respectively.

For the low mass flow rate (i.e., 0.1 g/s), the outlet pressure and temperature are around 172 bar and 199 K respectively with and without the distributed J–T effect. In this case, the drop in pressure of the high pressure fluid in the finned tube is low (around 8 bar) for a supply pressure of 180 bar. As a result, the pressure profiles with and without the distributed J–T effect overlap each other as seen in Figure 3a. The same is true for temperature profiles in Figure 3b. This is due to the fact that the changes in temperature due to the changes in pressure (second term of equation (1)) are negligible when the pressure drop is low. However, the pressure and

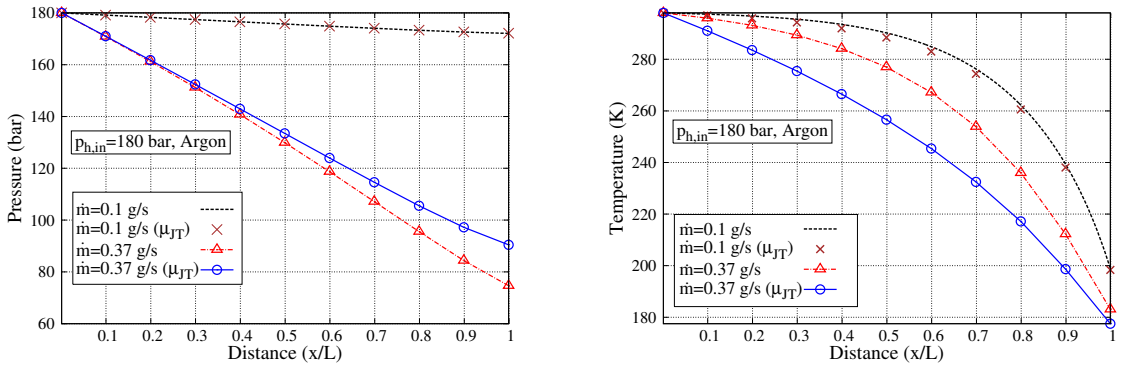

(a) (b)

Figure 3. Fluid in the finned tube: a) pressure [13]; b) temperature [13].

temperature profiles differ significantly when the mass flow rate increases to 0.37 g/s. The outlet pressure and temperature with the distributed J–T effect are 90 bar and 177.49 K respectively. The same without the distributed J-T effect are 74 bar and 183 K respectively. The pressure drop is of the order of around 90-100 bar over the length of the high pressure fluid in the finned tube as seen from Figure 3a. Therefore, the changes in temperature due to changes in pressure, represented by the second term in equation (1), become significant. When the distributed J–T effect is considered, the temperatures along the length of the fluid in the finned tube are lower as shown in Figure 3b. Due to this reason, the gas density is higher and the pressure drop is less when the distributed J–T effect is considered. Thus, the mathematical model is able to regulate the contribution of the distributed J–T effect with the mass flow rate.

4.2. Cooling effect

Figures 4a and 4b show the variation of cooling effect at 110 K for different mass flow rates and inlet pressures with and without the distributed J–T effect. Argon is used as the working fluid for all the cases. When the distributed J–T effect is taken into account, as shown in Figure 4a, the cooling effect increases linearly with the mass flow rate. This is because, in addition to the increase in the product $\dot{m}\triangle h$, the pressure drop increases with mass flow rate. This results in lower temperature before expansion. It is observed in Figure 4a that an increase in the mass flow rate from 0.1 g/s to 0.28 g/s increases the cooling effect from 2.3 W to 6.0 W for a supply pressure of 140 bar. Also, the cooling effect increases with supply pressure. When the supply pressure is raised from 140 bar to 220 bar, the cooling effect at 110 K for a mass flow rate of 0.24 g/s increases from 5.35 W to 8.07 W.

When the distributed J–T effect is not considered, a completely different trend is observed as shown in Figure 4b. As the mass flow rate is increased, the cooling power increases, reaches a maximum value, and then shows a decreasing trend. This observation is identical for all inlet pressures. As the mass flow rate increases, the heat transfer coefficient increases resulting in lower temperatures and higher cooling effect. Also the product $\dot{m}\triangle h$ increases. However, after a certain value of mass flow rate, the pressure drop increases and the gas at the exit of the finned tube expands from a lower pressure. This reduces the cooling effect. Here too, the cooling effect increases with supply pressure. Also, the mass flow rate at which the peak cooling effect is achieved increases with supply pressure. For a supply pressure of 140 bar maximum cooling effect of 3.2 W is obtained for a mass flow rate of 0.2 g/s. The maximum cooling effect at 220 bar is obtained with a mass flow rate of 0.345 g/s and is 8.23 W.

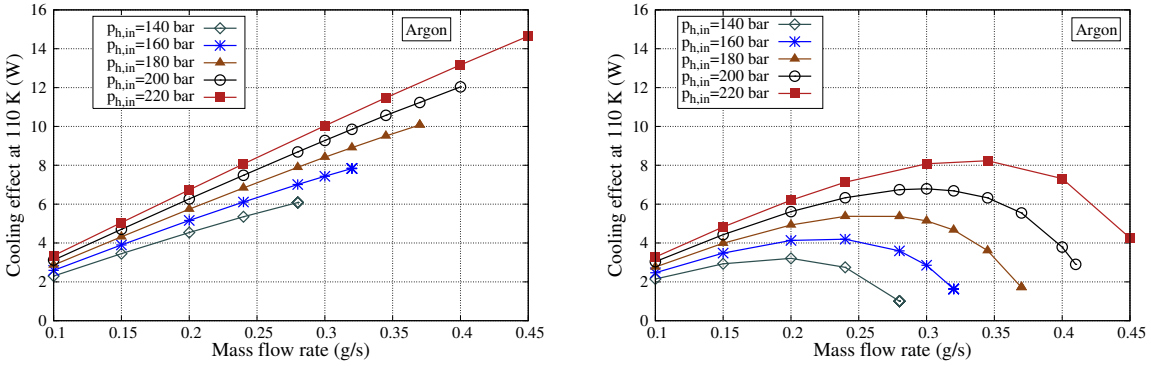

Figure 4. Cooling effect: a) with distributed J-T effect; b) without distributed J-T effect.

The cooling effect for a given mass flow rate is higher when the distributed J–T effect is considered. For an intermediate pressure of 180 bar, the cooling effects with 0.28 g/s, are 7.89 W and 5.37 W with and without the distributed J–T effect respectively. It can be observed from Figure 4a and 4b that the cooling effect, with and without the consideration of distributed J–T effect, is comparable for low mass flow rates. This is due to the lower contribution of the second term of equation (1) as observed in Figure 3.

4.3. Cool down time

Figures 5a and 5b, respectively, show the variation of cool down time with and without distributed J–T effect for different inlet pressures and mass flow rates. With the distributed J–T effect, as shown in Figure 5a, the cool down time reduces with increasing mass flow rate. This is obvious as cooling effect increases with the increasing mass flow rate. For a supply pressure or 140 bar with the distributed J–T effect, the cool down time reduces from 44.37 s to 24.88 s when the mass flow rate increases from 0.1 g/s to 0.28 g/s. The cool down time also reduces with an increase in supply pressure which is more pronounced at lower mass flow rates. For a mass flow rate of 0.2 g/s, raising the supply pressure from 140 bar to 220 bar reduces the cool down time from 31.42 s to 23.84 s.

Figure 5b shows the cool down time without the distributed J–T effect consideration. When the mass flow rate increases the cool down time first reduces, reaches a minimum value, and increases thereafter. The maximum cooling effect and minimum cooling time are obtained only for a optimum mass flow rate. Such a behaviour can be explained by noting that, initially, due to low mass flow rates, the heat transfer coefficients are also low. Therefore, more time is needed to reach the steady state if the heat capacity of the heat exchanger remains constant. With increased mass flow rate, the heat transfer coefficients increase and the cool down time reduces. Further increase in mass flow rate increases the pressure drop which in turn reduces cooling effect. This results in increase of the cool down time. The cool down time is comparable with and without the distributed J–T effect until the mass flow rate corresponding to minimum cool down time without distributed J–T effect is reached.

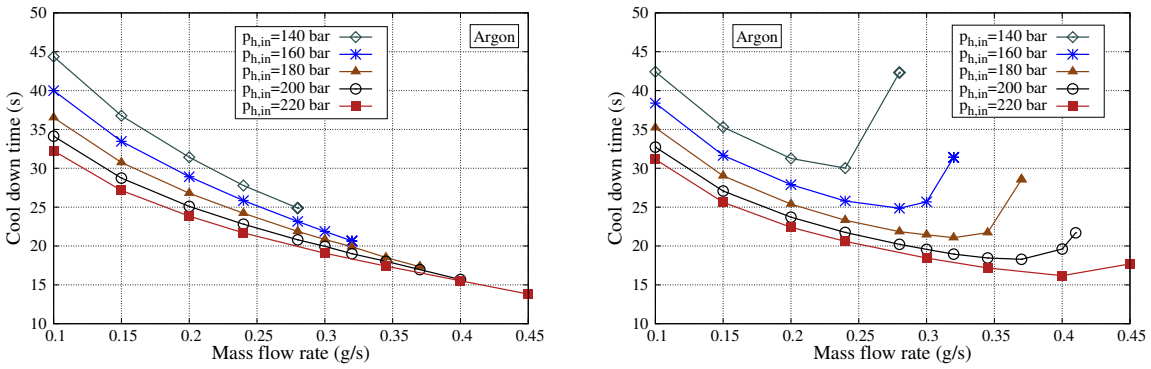

Figure 5. Cool down time: a) with distributed J-T effect; b) without distributed J-T effect.

4.4. Effect of working fluid

Normally, argon and nitrogen are used as working fluids for miniature J–T cryocoolers. Cooling capacity at 110 K and 180 bar with argon and nitrogen with and without distributed J–T effect is shown in Figure 6. For both the gases, the cooling effect is higher considering the distributed J–T effect and the trends of the cooling curves are similar. It is observed that the cooling capacity at 110 K is higher with argon as compared to nitrogen. With the distributed J–T effect, for an intermediate supply pressure of 180 bar and a mass flow rate of 0.28 g/s, the cooling effect with nitrogen is lesser by 1.33 W as compared to argon. Without the distributed J–T consideration, when compared with argon, the cooling effect with nitrogen is lesser by 2.96 W. This is because of the different thermo-physical properties of these gases. For inlet conditions of 298 K and 180 bar, the temperature and pressure before expansion for argon are 189 K and 128 bar respectively with the distributed J–T effect. The same for nitrogen are 165 K and 102 bar respectively. After expansion, corresponding to the above conditions before expansion, argon attains a two-phase state. The same is not true for nitrogen. Therefore, more cooling effect is obtained due to latent heat of vaporization. This observation conforms with the calculations [5] wherein it was found that the ideal cooling capacity of the J–T cryocooler with argon is more than that for nitrogen

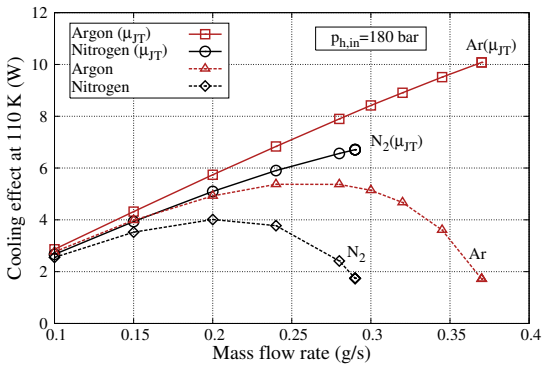

Figure 6. Cooling effect at 110 K with and without distributed J–T effect.

for the same operating range of temperatures and pressures.

5. Conclusions

In this work, the effect of mass flow rate and supply pressure on the performance of a miniature J–T cryocooler with and without the distributed J–T effect is studied. A one-dimensional transient model is employed for the numerical analysis. Cases with different supply pressures and mass flow rates are simulated with both argon and nitrogen as working fluids. The physical properties of these gases are evaluated at the local temperature and pressure conditions. Axial conduction is also taken into account for the solid elements.

The distributed J–T effect, over the finned tube length, is considered in addition to the J–T expansion at the end of finned tube. The distributed J–T effect cannot be neglected when the pressure drop over the finned tube length is large. The numerical model is able to regulate the contribution of the distributed J–T effect with mass flow rate. It is observed that the distributed J–T effect is significant when the mass flow rates are high. This is because the pressure drop increases with mass flow rate and therefore its contribution to enthalpy changes. As the mass flow rate are high during the initial period of cool down in J–T cryocooler, the contribution of distributed J–T effect will be very important during this period.

When the distributed J–T effect is considered, an increase in mass flow rate leads to a monotonic increase in the cooling effect. In this case, the cool down time reduces almost linearly. There is no optimum mass flow rate with maximum cooling effect and minimum cool down time as in the case without the distributed J–T effect. In all cases the cooling effect increases and the cool down time reduces with an increase in the supply pressure. These observations hold for both argon and nitrogen as working fluids. Also, it is found that the cooling capacity at 110 K is higher with argon than with nitrogen as working fluid.

References

[1] Xue H, Ng K C and Wang J B 2001 Performance evaluation of the recuperative heat exchanger in on a miniature Joule–Thomson cooler *Appl. Thermal Engg.* **21** 1829-44.

[2] Ng K C, Xue H and Wang JB 2002 Experimental and numerical study on a miniature Joule–Thomson cooler for steady-state characteristics *Int. J. Heat and Mass Trans.* **45** 609-18.

[3] Chua H T, Wang X and Teo H Y 2006 A numerical study of the Hampson-type miniature Joule–Thomson cryocooler *Int. J. Heat Mass Trans.* **49** 582-93.

[4] Hong Y J, Park S J and Choi Y D 2008 A numerical study of the performance of a heat exchanger for a miniature Joule–Thomson refrigerator *Cryocoolers 15 Int. Cryocooler Conf.* ed S D Miller and R G Ross Jr.:(California) pp 379-86.

[5] Ardhapurkar P M and Atrey M 2014 Performance optimization of a miniature Joule–Thomson cryocooler using numerical model *Cryogenics* **63** 94-101

[6] Chou F C, Pai C F, Chien S B and Chen J S 1995 Preliminary experimental and numerical study of transient characteristics for Joule–Thomson cryocooler *Cryogenics* **35** 311-16.

[7] Chien S B, Chen J S and Chou F C 1996 A study on the transient characteristics of a self-regulating Joule–Thomson cryocooler *Cryogenics* **36** 979-84.

[8] Hong Y J, Park S J, Kim H B and Choi Y D 2006 The cool-down characteristics of a miniature Joule–Thomson refrigerator *Cryogenics* **46** 391-95.

[9] Hong Y J, Park S J and Choi Y D 2010 A numerical study on operating characteristics of a miniature Joule–Thomson refrigerator *Superconductivity and Cryogenics* **12** 41-5.

[10] Maytal B-Z 2014 Hampson's type cryocoolers with distributed Joule–Thomson effect for mixed refrigerants closed cycle *Cryogenics* **61** 92-6.

[11] Damle R M and Atrey M D 2015 Transient simulation of a miniature Joule–Thomson (J–T) cryocooler with and without the distributed J–T effect *Cryogenics* **65** 49-58.

[12] AspenONE V 7.1. Aspen Technology Inc, Burlington, MA 01803, USA; 2009.

[13] Damle R M and Atrey M D 2015 The cool-down behaviour of a miniature Joule–Thomson (J–T) cryocooler with the distributed J–T effect and finite reservoir capacity *Cryogenics* **71** 47-54.